Journal of Atmospheric Chemistry **20:** 141–162, 1995.

Methane Emissions from a Landfill Measured by Eddy Correlation Using a Fast Response Diode Laser Sensor

D. C. HOVDE[1], A. C. STANTON[1], T. P. MEYERS[2] and D. R. MATT[2]
[1]*Southwest Sciences, Inc., 1570 Pacheco Street, Suite E-11, Santa Fe, New Mexico 87505, U.S.A.*
[2]*National Oceanic and Atmospheric Administration, Atmospheric Turbulence and Diffusion Division, Oak Ridge, Tennessee 37831, U.S.A.*

(Received: 18 June 1992; in final form: 12 November 1993)

Abstract. We describe a fast response methane sensor based on the absorption of radiation generated with a near-infrared InGaAsP diode laser. The sensor uses an open path absorption region 0.5 m long; multiple pass optics provide an optical path of 50 m. High frequency wavelength modulation methods give stable signals with detection sensitivity ($S/N = 1$, 1 Hz bandwidth) for methane of 65 ppb at atmospheric pressure and room temperature. Improvements in the optical stability are expected to lower the current detection limit. We used the new sensor to measure, by eddy correlation, the CH_4 flux from a clay-capped sanitary landfill. Simultaneously we measured the flux of CO_2 and H_2O. From seven half-hourly periods of data collected after a rainstorm on November 23, 1991, the average flux of CH_4 was 17 mmol m^{-2} hr^{-1} (6400 mg CH_4 m^{-2} d^{-1}) with a coefficient of variation of 25%. This measurement may underrepresent the flux by 15% due to roll-off of the sensor response at high frequency. The landfill was also a source of CO_2 with an average flux of 8.1 mmol m^{-2} hr^{-1} (8550 mg CO_2 m^{-2} d^{-1}) and a coefficient of variation of 26%. A spectral analysis of the data collected from the CH_4, CO_2, and H_2O sensors showed a strong similarity in the turbulent transfer mechanisms.

Key words: Methane, carbon dioxide, flux, landfill, diode laser, eddy correlation.

1. Introduction

Levels of atmospheric methane are increasing at a rate near 1% per year (Bolle *et al.*, 1986). To understand more fully the causes for this rise, many studies have been undertaken to quantify the global sources and sinks of methane, but uncertainties in the methane budget remain large (Cicerone and Oremland, 1988; Khalil and Rasmussen, 1990; Crutzen, 1991). The sources of methane are many: anaerobic decay of organic matter generates CH_4 in a diversity of environments. Most of the research has focused on assessing CH_4 fluxes and associated processes for natural wetlands, tundra, rice paddies, biomass burning and enteric fermentation.

Landfills have been identified as significant anthropogenic sources of atmospheric CH_4 and are believed to account for 6 to 18% of the total CH_4 emissions (Bingemer and Crutzen, 1987). Quantitatively, this amounts to approximately 30×10^6 T/yr to 70×10^6 T/yr, with the majority of methane produced in the

industrialized nations because they generate a disproportionate amount of waste. The large uncertainty in the CH_4 emissions from landfills stems from uncertainties in the estimates of the type and amount of waste material, past and present landfill practices, and the role of CH_4 oxidizing microbes (Cicerone and Oremland, 1988). Few direct measurements of CH_4 emission rates from landfills have been reported in the open literature (Bogner and Vogt, 1991; Tohjima and Wakita, 1993).

The methane produced at landfills need not be released to the atmosphere. Landfill gas, chiefly methane and carbon dioxide, can be recovered from landfills for use directly in local electrical generators or as feedstock for producing natural gas. Estimates of CH_4 recovery rates range from 30 to 90% for systems in use today (Senior and Kasali, 1990). Landfill gas recovery can be economical, especially at more recent facilities. Recovery represents a possible method for significantly reducing global CH_4 emissions.

Even at strong sources such as landfills, methane is present in the atmosphere only in trace amounts, and the measurement of its flux is experimentally challenging. Both micrometeorological and chamber methods have been used to measure methane fluxes from natural sources. Soil diffusion and plume dispersion methods have been used to measure methane flux at landfills. In the soil diffusion experiment (Bogner and Vogt, 1991), gas samples were drawn at various depths in the soil and analyzed for methane content. Using the soil diffusion properties, the profile of concentration vs. sampling depth was modeled to extract a methane flux. This method gives detailed information about where in the soil the methane is generated (and where it is consumed), but it samples gas from a very small area. It is very sensitive to variations in soil transport and other inhomogeneities in the system under study; Bogner and Vogt (1991) report a wide range of methane fluxes as determined by this method. In a recent study (Tohjima and Wakita, 1993), atmospheric methane concentration profiles were measured by a flame ionization detector at distances of several kilometers downwind from a large landfill in Tokyo bay. Atmospheric plume dispersion models were used to compute the very high source emission rate, which averaged 200 g m^{-2} d^{-1}.

The widely used chamber methods have advantages that include low cost, high sensitivity, relative ease of implementation, and the variety of surfaces over which this technique can be applied. Disadvantages include intermittent measurements, suppression of the effects of atmospheric turbulence on gas exchange, and alteration of radiation, temperature, and humidity within the enclosure. Chambers measure the flux through a well defined surface, typically of the order of one square meter. Unfortunately, some methane sources are very inhomogeneous on this length scale. The landfill we studied exhibited large variations in emissions; after a rainstorm, we saw gas bubble out of numerous small vents. Because so many measurements are required, using chambers to determine the *average* flux from an inhomogeneous source quickly becomes tedious. Moreover, the possible measurement bias introduced by using chambers to assess fluxes has yet to be evaluated. Recently, Moore and Roulet (1991) compared CH_4 emission rates from a static chamber

with those from a co-located dynamic enclosure. From their comparison, the fluxes derived from the static chambers were on average 20% lower than those obtained from dynamic chambers. Despite these drawbacks, until recently only chamber techniques were used to measure CH_4 emission rates.

Eddy correlation is a micrometeorological method which can provide continuous, direct measurement of unperturbed CH_4 exchange rates. By rapidly measuring both the instantaneous concentration, c_i, and vertical wind velocity, w_i, the vertical turbulent flux can be determined as

$$F_c = \frac{1}{n}\sum_{i=1}^{n}(w_i - \langle w\rangle)(c_i - \langle c\rangle). \tag{1}$$

The bracketed quantities denote an average which is subtracted from the instantaneous values. Atmospheric turbulence naturally provides an integrated average of the flux from a 'footprint' upwind of the sensors, with dimensions of hundreds of square meters. For methane, as with many other trace species, the application of this method has been limited by the availability of fast response sensors. Recently, three research groups have devised fast methane sensors using mid-infrared lasers. Instruments using lead salt lasers have been applied to measure fluxes in a suburban research park (Zahniser *et al.*, 1987; Anderson and Zahniser, 1991) and a northern peatlands (Verma *et al.*, 1992; Hastie *et al.*, 1983), and in airborne measurements as part of the NASA GTE/ABLE experiment in Alaska (Sachse *et al.*, 1991; Ritter *et al.*, 1992). A Zeeman-split helium neon laser at 3390 nm has been reported by McManus *et al.* (1989) and used in ground based measurements during GTE/ABLE (Fan *et al.*, 1992).

Near-infrared absorption features can also be used for fast response monitoring of methane concentrations (Mohebati and King, 1988; Shimose *et al.*, 1991; Uehara and Tai, 1992). These features, which arise due to vibrational overtones or combinations, have smaller cross sections for absorption than mid-infrared fundamentals, but this drawback is offset by several practical advantages unique to this wavelength region. Single frequency near infrared diode lasers and high quantum efficiency detectors have been engineered for fiber optic communication applications. These components feature room temperature operation, small size and weight, low power requirements, and high reliability. Commercial InGaAsP distributed feedback (DFB) near-IR diode lasers can be fabricated in the 1200 to 1700 nm wavelength region; single mode output power of several mW is typical. Detection techniques based on high frequency modulation of the laser current yield sensitivities for measuring 1 part in 10^6 absorbance or smaller (Bomse *et al.*, 1992).

At Southwest Sciences, we have developed a fast response methane sensor based on the absorption of radiation from a 1650 nm single mode InGaAsP diode laser. With low power requirements, and free from cryogenic coolants, this sensor is well suited for field use. High frequency wavelength modulation methods were used to lock the laser to the absorption feature while continuously measuring

the absorbance. We evaluated the accuracy and stability of the instrument in our laboratory. We then tested the instrument in the field in a one week experiment to measure the methane flux from a landfill near the NOAA laboratory in Oak Ridge, Tennessee. Although measurements were made on the last two days, the calibrated data presented here were obtained only on the last day. As expected, the landfill was a strong source of methane, emitting an average flux of 17 mmol m^{-2} hr^{-1} (6400 mg m^{-2} d^{-1}). Simultaneously we measured the flux of sensible heat, H_2O, and CO_2. Power and co-spectral statistics are presented to evaluate the sensitivity and response characteristics of the CH_4 sensor. Statistical methods are also used to estimate the lowest CH_4 flux that can be detected with the current sensitivity and noise characteristics.

2. Experimental Procedures

2.1. SITE DESCRIPTION

A one week experiment (18–23 November, 1991) was conducted at a sanitary landfill located near the U.S. Department of Energy's (DOE) Y-12 facility in Oak Ridge, Tennessee, U.S.A. The landfill is generally rectangular area with dimensions of 350 m by 190 m. The landfill is uniformly covered with at least 45 cm of native soil-clay mixture. The waste buried in the landfill consists mostly of paper products, packaging material, and food waste from plant cafeterias. At the time of the experiment, the area was covered with biologically dormant grasses. The instrumentation was located on a telescoping mast at a height of 2.5 m, situated roughly in the middle of the landfill. A mobile home unit equipped with a 5 kW generator was located approximately 35 m north of the tower. At times during the week, wind shifts brought generator exhaust to the tower, resulting in spikes in the CO_2 and H_2O levels, but this did not occur during the measurement period we report here.

2.2. METHODOLOGY AND INSTRUMENTATION

The eddy correlation method was employed to measure the turbulent exchange of sensible heat, H_2O, CO_2, and CH_4 between the atmosphere and the landfill. The application of the eddy correlation method requires fast response instrumentation to measure the three components of the wind vector and the scalars of interest (see Businger, 1986; Baldocchi *et al.*, 1988). A three-dimensional sonic anemometer (Kaimal *et al.*, 1990) was used to measure the components of the wind vector and virtual temperature. Fast response measurements of H_2O and CO_2 were made with an open-path, infrared absorption gas analyzer (Auble and Meyers, 1992); the methane instrument is described below. Other standard meteorological measurements included wind speed and direction, air temperature, relative humidity, solar and net radiation, soil temperatures at three depths (2, 4, and 6 cm), and the ground

surface temperature. The heat conduction rate into the soil was determined with ground heat flux plates inserted at a 1 cm depth.

2.3. DIODE LASER METHANE SENSOR

The methane sensor was designed to provide fast response with $\sim 1\%$ accuracy for ambient methane, in a lightweight, low power package. The instrument consists of a diode laser and control electronics, the optical probe, detection/demodulation electronics, and a portable computer. A near infrared distributed feedback diode laser operating at 1650 nm was selected due to its low power, room temperature operation, and single mode output. The laser wavelength can be tuned by controlling the temperature ($d\lambda/dT = 0.1$ nm/K) and current ($d\lambda/dI = 6 \times 10^{-3}$ nm/mA). The bandwidth for current tuning is near 1 GHz. To achieve the required sensitivity, we used high frequency wavelength modulation methods (Silver, 1992; Bomse, 1991; Bomse *et al.*, 1992). The optical probe was a Herriott style multiple pass cell (Herriott *et al.*, 1964) open to the atmosphere. The open path approach for eddy flux measurements permits the use of large mirrors, and hence a large number of passes, without introducing time delays or time response limitations that occur when air is sampled through a closed cell, and without the need for vacuum pumps.

2.3.1. *Theory*

The near infrared diode laser sensor measures methane by absorption of the R(2) rotational line in the $2\nu_3$ overtone band of $^{12}CH_4$ near 1650 nm (Shimose *et al.*, 1991; Uehara and Tai, 1992). Spectral parameters for this band are well known (Varanasi, 1971; Bobin, 1972; Darnton and Margolis, 1973; Margolis, 1973; Sarangi and Varanasi, 1974; Fox *et al.*, 1980). At atmospheric pressure, this line is Lorentzian with a width of approximately 0.03 nm. The laser sensor is based on the use of high frequency wavelength modulation techniques to quantify small, wavelength dependent power changes due to this spectrally narrow absorption feature. We briefly review those aspects important to understanding the sensitivity and accuracy of the methane flux results. From Beer's law, the absorbance may be written

$$\frac{I(\lambda)}{I_0} = e^{-\alpha}\,, \tag{2}$$

where the optical depth α is given by

$$\alpha = \sigma(\lambda) n \ell + \text{baseline}(\lambda) \tag{3}$$

$$= S\, G(\lambda) n \ell + \text{baseline}(\lambda)\,. \tag{4}$$

Multiple pass optics were used to achieve an optical path length ℓ of 50 m. The methane number density n is the quantity to be determined. In Equation (4), the

cross section σ is shown as the product of the line strength, S, and a normalized lineshape function, $G(\lambda)$, that contains the wavelength dependence. Pressure broadening dominates $G(\lambda)$, which can be approximated as a Lorentzian with half-width at half maximum γP_{total} (γ is the pressure broadening coefficient). Both S and $G(\lambda)$ are temperature dependent, and $G(\lambda)$ depends also on gas pressure and composition. In the absence of modulation effects, the peak absorbance depends only on the mixing ratio of methane, and is about 2×10^{-3} for ambient methane; increasing the pressure of all gases increases only the spectral width of the feature, but not the peak absorbance. Finally, we include an explicit wavelength dependence for the baseline transmission even in methane-free air.

In order to determine the methane concentration, we must estimate the background function and measure the laser power, I_0. In addition, the laser power is contaminated by excess '$1/f$' noise. We reduce the effects of excess noise and slowly varying background terms by modulating the wavelength of the laser at two frequencies (Bomse, 1991):

$$\lambda(t) = \lambda_0 + \Delta \sin(\Omega t) + \delta \sin(\omega t)\,, \tag{5}$$

then stepwise demodulating at $4\Omega = 20$ MHz, then $2\omega = 20$ kHz to measure the methane concentration. The resulting signals – our measurement of α – *are* pressure dependent. The pressure dependence has not yet been investigated experimentally for our instrument, and a theoretical expression for the doubly demodulated signal has not been presented in the literature. However, for the corresponding case where only a single modulation frequency ω is applied, the theory was worked out by Arndt (1965). The singly demodulated signal is given by a Chebychev integral that depends on the ratio of the wavelength modulation amplitude, δ, to the pressure dependent line width, γP. This integral must be evaluated numerically, but two cases are worth noting: when $\delta/\gamma P \ll 1$, the signal at $k\omega$ is proportional to $(\delta/\gamma P)^k$, and the signal reaches a maximum for $\delta/\gamma P = 2.2$ (if $k = 2$) or 3.9 ($k = 4$) (Silver, 1992).

We expect that the results of Arndt (1965) can be generalized to describe the dual modulation and demodulation used here. We have observed that the signal amplitude behaves approximately as the product of the amplitudes expected for each one dimensional demodulation step. We therefore estimate the effects of small modulation induced changes on the measured value of α by expanding each of the one dimensional Chebychev integrals, C_1 and C_2, in a Taylor series in $m = \delta/\gamma P$ or $M = \Delta/\gamma P$. Keeping the linear terms only gives

$$\frac{\Delta\alpha_{\text{exp}}}{\alpha_{\text{exp}}} = \frac{d\,\log C_1}{d\,\log m}\frac{\Delta m}{m} + \frac{d\,\log C_2}{d\,\log P}\frac{\Delta M}{M}\,. \tag{6}$$

The required derivatives can be found from a log-log plot of signal vs. modulation index (Figure 1). The slope varies from $+4$ to -1 for the 4Ω demodulation, and from $+2$ to -1 for the 2ω demodulation.

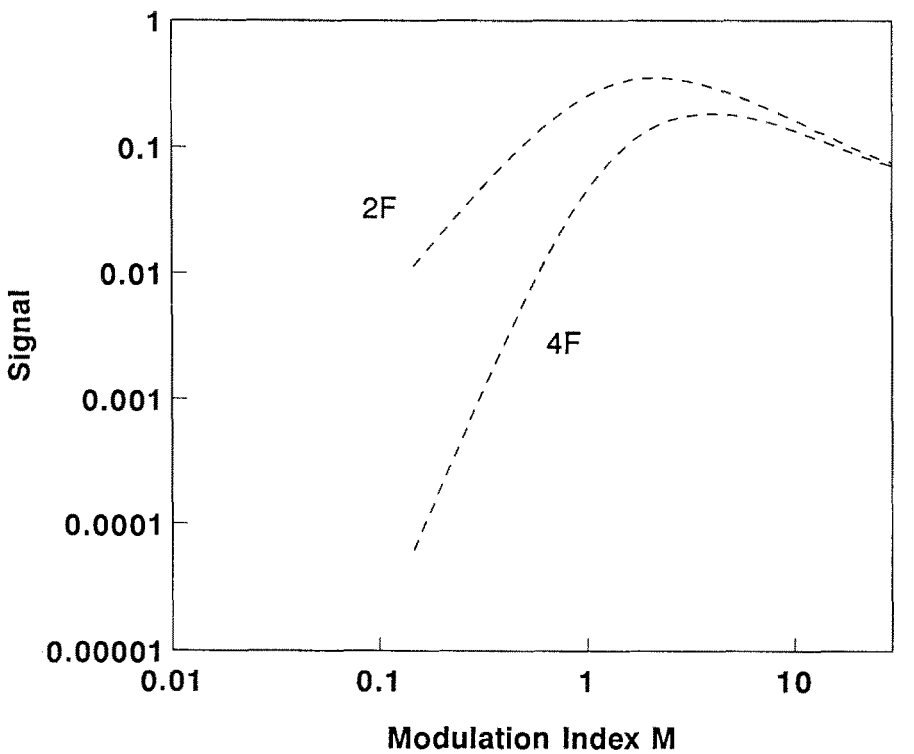

Fig. 1. Maximum demodulated harmonic signals calculated for a Lorentzian pressure-broadened absorption line. The horizontal scale is the ratio of the modulation amplitude to the linewidth, see text. The vertical scale is normalized by the peak absorbance of an unmodulated, optically thin Lorentzian.

Although laser power changes of 3×10^{-7} in a 1 Hz bandwidth have been detected in our lab by high frequency wavelength modulation methods, instabilities in the baseline function in many cases limit the sensitivity that can be achieved. This baseline arises in part from inherent nonlinearities in the laser output power (Uehara and Tai, 1992), and in part from weak interference fringes from stray reflections in the optical path. Such fringes are difficult to eliminate, since a stray reflection with power of 10^{-8} of the main beam will produce an etalon of 10^{-4} amplitude, as is easily verified by remembering that optical power is proportional to the square of the electric field. Several schemes for reducing interference effects have been developed (Cassidy and Reid, 1982; Webster, 1985; Cooper and Carlisle, 1988; Silver and Stanton, 1988). We did not use etalon suppression in our preliminary test. Instead we observed that lower values of the modulation amplitude gave the optimum signal/background ratio, so we simply reduced the modulation amplitudes below those which gave maximum signals. Further development of the instrument is aimed at reducing or stabilizing the optical interferences to permit the use of a higher modulation amplitude, and hence optimum sensitivity, without baseline drift.

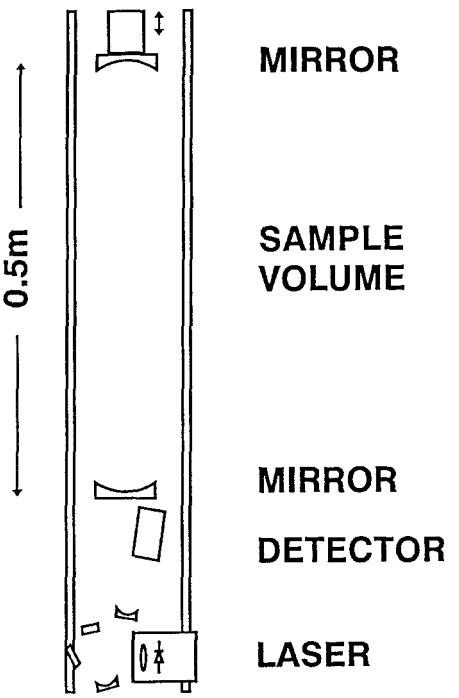

Fig. 2. Physical configuration of the methane sensor. The upper mirror is mounted on a translation stage. Small beam steering mirrors, not labeled in the figure, direct the laser into the multiple pass region, and focus the output onto the photodetector. A clamp at the top of the vertical rods holds the sensor on the meteorological tower.

2.3.2. *Physical Configuration*

Figure 2 shows the methane sensor. A vertical open path multiple pass cell (Herriott *et al.*, 1964) consisting of two 10 cm diameter mirrors defined the sample volume. The mirrors were ground with a 60 cm radius of curvature, dielectric coated for high reflectivity, and spaced about 50 cm apart to give 106 passes through the sample region. The number of passes was determined by measuring, for several settings of the Herriott cell, both the mirror spacing and the optical path induced phase shift of the 5 MHz modulation carrier frequency. The base path length was chosen to give good high frequency response for moderate vertical wind speeds. A hole in the lower mirror (5 mm diameter, 1 cm from the mirror edge) was used to couple the laser beam into and out of the cell. An RF shielded box mounted 25 cm below the lower mirror housed the laser. The 1 mm diameter InGaAs detector and its transimpedance preamplifier were mounted 10 cm below the lower mirror; a 25 mm focal length mirror directed the light onto the detector. The DC and high frequency components of the photocurrent were both available from the preamplifier.

The multipass cell, laser and detector were mounted on an open frame of 3/8″ steel rods; this package was 110 cm high, less than 30 cm wide, and weighed 7 kg. Commercial optical breadboard mounting hardware was used to position the laser and mirrors. The upper mirror was mounted on a translation stage to permit fine adjustment of the mirror spacing; sub-millimeter adjustments were necessary to obtain large numbers of passes. A photograph of the instrument has appeared elsewhere (Stanton and Hovde, 1992).

The electronic layout is shown in Figure 3. The laser was powered by a low noise current supply, ILX Lightwave model LDX 3620. The laser temperature was stabilized by two stages of thermoelectric cooling to about 0.01 °C. Active locking of the laser wavelength to the center of the methane transition was accomplished using the integrated error from the atmospheric methane signal, with the techniques described by Bomse (1991). The error signal was summed with a 10 kHz sine wave modulation and impressed onto the laser current through the modulation port of the current supply. High frequency wavelength modulation at 5 MHz, generated from the internal oscillator of a Palo Alto Research model PAR 100 lock-in extender, was coupled via a Pi-type filter directly onto the laser. A portion of the 5 MHz sine wave was upconverted to 20 MHz and used as the local oscillator in the PAR 100 for the first demodulation step. The PAR output was sent to two commercial lock-ins for demodulation, one set at 10 kHz to provide the line-locking signal, and the other referenced to 20 kHz to provide the signal proportional to methane concentration times laser power (Bomse, 1991). Support electronics were located remotely at the base of the tower and in a trailer 30 m downwind. The power consumption for the instrument, including all support electronics and the laptop computer, was about 200 W at 120 Vac, 60 Hz. Significant reduction in power consumption will be possible through the use of custom detection electronics.

The 0.1 s, 6dB/octave time constant on each of the lock-ins filtered the error and concentration data prior to 16 bit digitization at 10 Hz. A portable computer (Toshiba T3200SX) equipped with an analog interface (Data Translation DT2805/5716A) logged the data for later analysis, integrated the wavelength locking error signal, and formed the ratio of the 20 kHz demodulated signal to the DC photocurrent. This ratio, which represents our estimate of the instantaneous methane concentration, was put out as an analog voltage to the micrometeorological data acquisition system described below. Our choice of time constant limited the high frequency response. We have since implemented analog division with a bandwidth of 50 Hz that should improve the high frequency phase and amplitude response of our sensor.

2.4. CALIBRATION AND SENSITIVITY OF THE METHANE SENSOR

When testing or calibrating the sensor, we enclosed the 4ℓ sample region and flowed known mixtures of methane diluted in dry air (36 ppm in the lab, 2 ppm in the field) and dry, zero air at a total flow rate of 10 ℓ min^{-1}. The work-up of these data,

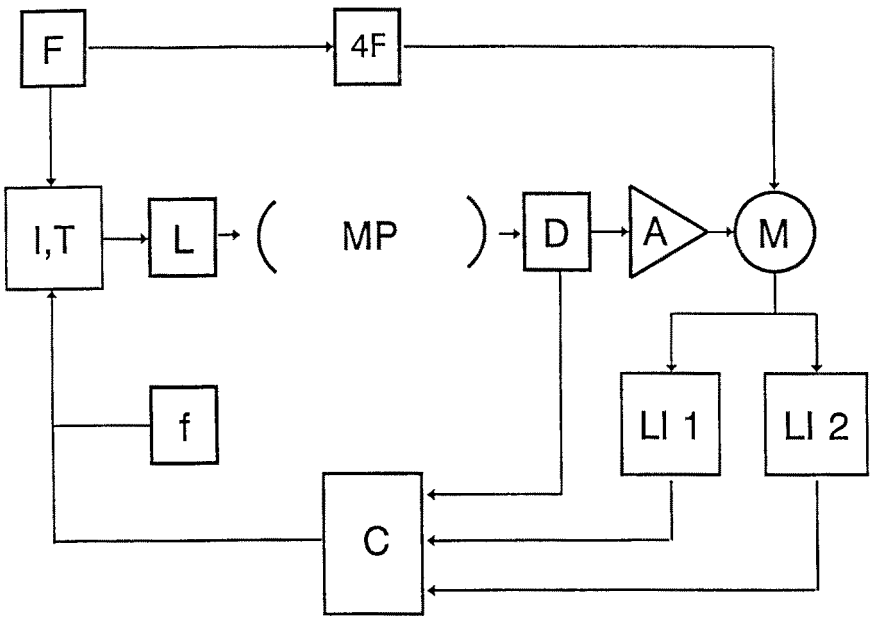

Fig. 3. Electrical schematic for laser control and signal processing, showing the laser current and temperature control units (I, T), high frequency modulation source (F) and frequency quadrupling (4F), low frequency modulation source (f), laser (L), multipass cell (MP), photodiode detector (D), transimpendance preamplifier (A), mixer (M), wavelength feedback lock-in at 10 kHz (LI 1), methane amplitude lock-in at 20 kHz (LI 2), and portable computer and A/D-D/A interface (C). The computer monitors the DC photocurrent and the output of the two lock-ins, and generates a correction to the laser current.

Figure 4, demonstrates that the signal is linear in concentration, but with a non-zero offset. This offset is due in part to nonlinearities in the laser power response (Uehara and Tai, 1992) and in part to broad optical interference fringes, and it is associated with the relatively large wavelength modulation amplitude needed for optimum detection sensitivity of atmospheric pressure broadened signals.

Data acquired in the lab with a constant methane composition were used to determine the Allan variance of the system (Allan, 1966; Werle *et al.*, 1991). The noise showed a minimum at 0.1 Hz averaging bandwidth, but appeared fairly flat out to 0.03 Hz, the lowest frequency analyzed. No changes in the noise level were noted in the field. Our eddy correlation results indicate that frequencies in the range 0.008 to 0.3 Hz contribute most of the flux. Noise in this bandwidth is about 65 ppb and is roughly independent of bandwidth. The sensitivity of our field instrument approaches that expected by scaling the laboratory results of Uehara and Tai (1992) up to our 50 m pathlength. They obtained a $S/N = 1$ detection limit of 0.3 ppm-m over a path of a few meters.

Eddy correlation provides good rejection for any noise source that is uncorrelated to vertical wind. However, measurement errors in the methane concentration that

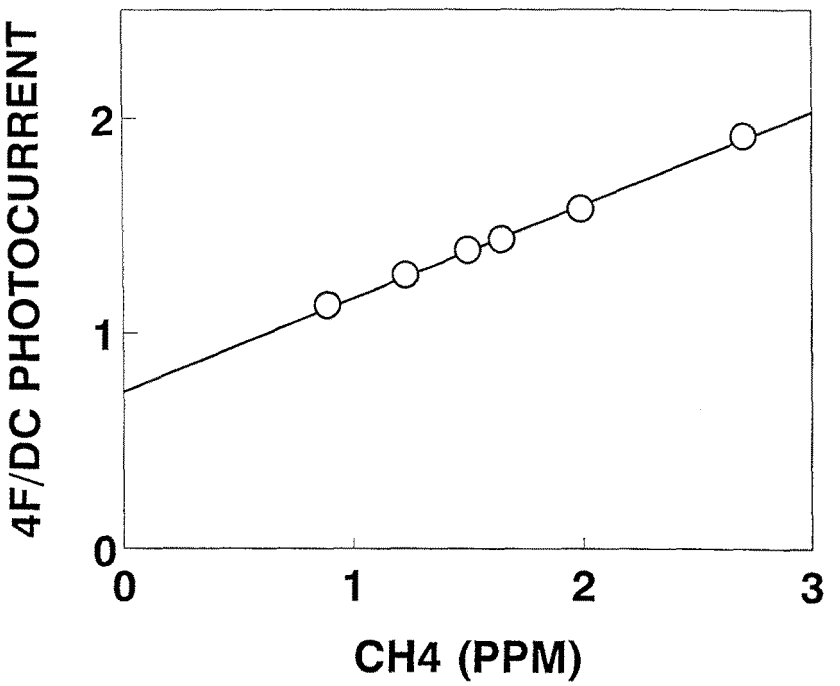

Fig. 4. Laboratory calibration of the methane flux sensor, obtained by flowing dry, methane free air and a 36 ppm methane/dry air standard. A significant intercept is evident, which may be due to optical effects (see text). Eddy correlation measurements are sensitive to changes in concentration and so depend on the slope of the line.

correlate with vertical wind speed will appear as systematic errors in the observed flux. These error sources should be distinguished from the corrections for humidity and temperature that are applied even to an ideal sensor (Webb, 1980). Because temperature, water vapor and carbon dioxide concentrations also correlate with vertical wind, possible systematic errors include the effects of temperature on the line strength, effects of Lorentzian wings of nearby H_2O or CO_2 lines, changes in the methane pressure broadened linewidth due to changes in temperature, pressure, or gas composition, and instrumental factors such as wind or temperature dependence of optical alignment. When the spectral parameters are well known, the effects of some of these changes can be estimated from Equation (6). Table I collects our estimates for systematic methane flux errors due to changes in the line strength and line width due to temperature. These systematic errors are of the same order of magnitude as the ideal gas correction for mass flux, shown for comparison. To estimate the flux error we have assumed constant pressure, typical values of $\sigma_T = 0.5$ K and $\sigma_w = 0.5$ m/s, and the temperature flux $F_T \approx 0.35\sigma_T\sigma_w$. Increases in temperature decrease the integrated line strength, S, but also decrease the linewidth, γP. The change in the observed signals depends on the modulation amplitude. In the limit of small modulations (Δ, $\delta \ll \gamma P$), the linewidth depen-

TABLE I. Systematic errors due to temperature dependence of line width and strength, and ideal gas correction for mass transport. The linewidth term is evaluated for both small and optimum modulations, using the approximate theory of Section 2.3

Systematic flux errors [mg m^{-2} d^{-1}]	Low modulation	Optimum modulation
Line width	140	0
Line strength	–32	–32
Ideal gas	–28	–28
Total	80	–60

dence dominates, but its contribution goes smoothly to zero when Δ and δ are set to their optimum values. *The proper choice of modulation amplitude can eliminate (to first order) systematic errors introduced by temperature fluctuations.* We used modulation amplitudes somewhat below the optimum values, and so may have obtained partial cancellation of the temperature dependent errors.

The linewidth of the methane transition also is a function of gas composition, due to the different efficiencies of various gases for pressure broadening (Darnton and Margolis, 1973; Varanasi, 1971). The importance of this effect on eddy correlation measurements was studied by Lubken *et al.* (1991), who measured the broadening of several mid-infrared methane absorption lines by various gases. For small methane flux and large water flux, this effect was expected to cause systematic errors from 1 to 10% of the true methane flux. The pressure broadening of the methane $2\nu_3$ band by water has not been measured, so we are not able to estimate the effect on the large flux we measured.

The HITRAN compilation of infrared line parameters lists several weak H_2O and CO_2 lines in the region of the methane R(2) rotational transition. Calculations based on these tables indicate that our false signals from water vapor are 5×10^{-5} smaller than the methane peak. Consistent with this, preliminary lab tests showed no effect by water or CO_2 lines on the amplitude of the methane signal, at least for the large fluxes measured at a landfill. For measuring smaller methane fluxes, more extensive tests are needed to quantify this possible systematic error and, if necessary, to identify which methane absorption lines are least affected. Alternatively, the output of fast response temperature and water vapor sensors, e.g. Auble and Meyers (1992), could be used to make real time corrections to the methane concentration. Such instrumentation is needed anyhow to make the corrections described by Webb (1980).

2.5. DATA ACQUISITION

Data from the fast response sensors were sampled and digitized at 10 Hz using a 12 bit analog to digital system associated with the sonic anemometer, and then transmitted to a portable microcomputer (separate from the computer associated with the methane instrument) housed in the mobile home unit via RS-232 serial

communication protocols. The computer continuously displays the incoming raw data in a strip-chart like fashion. All data were written to portable storage media for post-processing.

The mean values of the wind speed and scalars (the bracketed quantities in Equation (1)) were estimated in real time using a digital recursive filter (200 s time constant). A 30 min averaging period was used in the computation of the flux which resu lts in 1.8×10^4 samples acquired at 10 Hz. At the end of each 30 min run, the average vertical velocity at perfectly flat sites should be approximately zero and the covariance of the vertical velocity with the measured concentrations is a turbu lent flux that is normal to the mean wind streamline. For experimental sites that are not perfectly flat, the measured w is not always equal to zero. However, the coordinate system of the sonic anemometer can be mathematically rotated to obtain a zero mean vertical and transverse velocity ($\overline{w} = \overline{v} = 0$). This is the usual practice to correct for small misalignment errors of the sonic anemometer as well as to determine the mean vertical turbulent flux normal to the horizontal streamlin es of airflow, which generally follows the contours of the land. The vertical rotation angle was about 3° for the data reported here.

3. Results

3.1. SURFACE ENERGY BUDGET

For all eddy flux measurements, several criteria are used to assess whether the measured fluxes at some specified height above the surface are representative of the surface itself (Hicks *et al.*, 1989). The closure of the surface heat budget is most often used to assess the adequacy of a site for interpretation of micrometeorological measurements. If the measurements made at some height above the surface *are* representative of the surface, then the local measurements of net radiation (R_n), ground heat flux (G), and heat storage (S) should equal the sum of sensible (H) and latent heat (LE) fluxes measured above the surface. The ground storage terms were determined from known heat capacities and changes in soil temperature for each averaging period. Figure 5 compares the available energy ($R_n - G - S$) with the measured sensible and latent energy fluxes. The agreement is good, with a bias of the regression line that is not significantly different from zero. This indicates that the fluxes measured at 2.5 m above ground level are representative of the surface below.

3.2. METHANE AND CARBON DIOXIDE EMISSION RATES

Time lost to poor weather and spent in initial testing and setup allowed for only seven half-hourly periods of calibrated data to be processed from the prototype CH_4 sensor, all collected on November 23, 1991. Figure 6 represents a typical time seri es of the H_2O, CO_2, and CH_4 measurements. The high degree of correlation is indicative of the similarity of the respective turbulent transport processes. The

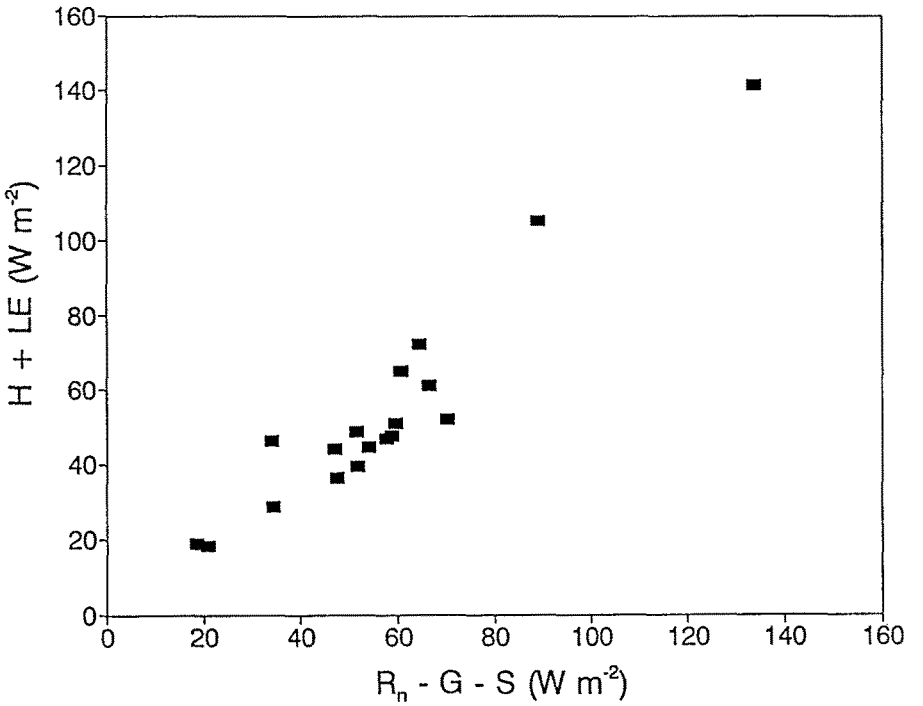

Fig. 5. Available energy (sum of the net radiation (R_n), ground heat flux (G), and ground storage (S)) versus the summation of sensible (H) and latent energy (LE) flux.

mean eddy fluxes along with other meteorological measurements are presented in Table II. For the seven consecutive periods, the average emission rates for CH_4 and CO_2 were 17 and 8.1 mmol m^{-2} hr^{-1}, respectively. The measured emission rate of CH_4 is twenty times greater than the fluxes measured over a northern peatland (Verma *et al.*, 1992), rice fields (Sass *et al.*, 1990) and subarctic boreal fens (Moore and Roulet, 1991; Moore and Knowles, 1990). When compared to recent eddy fluxes over subarctic tundra (Fan *et al.*, 1992), our measured CH_4 emission rates are $\approx$200 times larger. However, our measured fluxes fall at the low end of the wide range (1 to 14 000 mmol m^{-2} hr^{-1}) determined by subsurface diffusion at a landfill in Illinois (Bogner and Vogt, 1991). The estimates from the soil diffusion studies have associated uncertainties that span nearly two orders of magnitude because of uncertainties in the soil diffusion properties. In their plume dispersion study of a landfill in Tokyo bay, Tohjima and Wakita (1993) determined methane emissions to be in the range 390–650 mmol m^{-2} hr^{-1}, or about 30 times the flux measured in this work. This higher flux might be due to the warmer season (August for the Tokyo measurements, November for our own), or the amount or type of refuse.

The CH_4/CO_2 mole ratio of landfill gas resulting from anaerobic decomposition of biochemically degradable carbon is estimated to be 1 : 1 (Bingemer and Crutzen, 1987). Using measurements of gas concentrations at different soil depths within

TABLE II. Meteorological values and corresponding energy and mass fluxes from seven half hourly periods including the mean wind speed ($\overline{u}$), friction velocity (u_*), air temperature (T_a), relative humidity (RH), global (R_g) and net (R_n) radiation, soil temperature (T_s), ground heat flux (G), sensible (H) and latent energy flux (LE), and the flux of CO_2 (F_{CO_2}) and CH_4 (F_{CH_4})

Day	Time	$\overline{u}$	u_*	T_a	RH	R_g	R_n	$T_{s,\,6\,cm}$	G	H	LE	F_{CO_2}	F_{CH_4}
		[m/s]	[m/s]	[°C]	[%]	[W m^{-2}]	[W m^{-2}]	[°C]	[W m^{-2}]			[mmol m^{-2} hr^{-1}]	
326	1330	2.88	0.29	12.7	91	161	120	13.65	–6	40	58	6.4	18.4
326	1400	1.93	0.25	12.5	91	63	39	13.61	9	13	30	7.4	19.4
326	1430	2.01	0.27	12.7	90	94	66	13.64	3	21	45	11.5	21.4
326	1500	2.06	0.18	12.5	91	65	42	13.56	10	16	31	8.0	14.0
326	1530	2.13	0.26	12.4	88	78	52	13.54	9	18	41	8.3	16.6
326	1600	1.58	0.15	12.4	88	64	41	13.49	9	12	25	5.1	8.7
326	1630	1.03	0.10	12.4	88	50	26	13.46	8	6	20	9.9	17.6

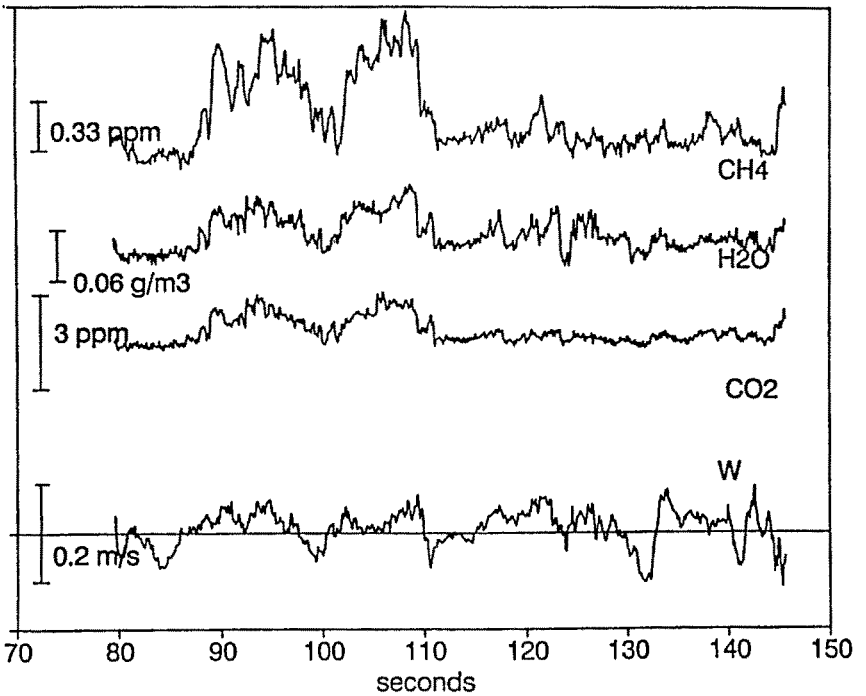

Fig. 6. A one minute time series showing similarity of the vertical wind velocity (w) and the concentrations of CH_4, CO_2, and H_2O.

a sanitary landfill area, Bogner and Vogt (1991) reported CH_4/CO_2 mole ratios ranging from 1.3 : 1 to 1.8 : 1. In the emitted gas, the ratio will be higher if CO_2 dissolves in the ground water. Soil moisture was not lacking during the time of our measurements because the ground was nearly saturated after receiving five centimeters of rain. The measured CH_4/CO_2 flux mole ratio of 2 : 1 is consistent with that expected of the emitted gases under these conditions.

3.3. POWER AND CO-SPECTRA

A spectral analysis was conducted on a segment of the continuously recorded data time series to evaluate possible noise contributions and assess the frequency response of the CH_4 sensor. A discrete Fourier transform was applied to four data segments, each consisting of 4096 samples. The resulting power- and co-spectral statistics from the CH_4 time series were averaged and compared against the simultaneous results from the time series of the H_2O signal from the infrared gas analyzer. The spectral estimates in Figure 7 were normalized by the associated variance for comparison. The CH_4 power spectral estimates are in close agreement with the spectral estimates from the H_2O signal from $n = 0.001$ Hz to $n = 0.8$ Hz. *Low frequency baseline drift is absent from the methane signal.* Above 0.8

Hz, the methane power spectral estimates decline faster than the expected –2/3 slope which is observed in the H_2O spectra. Likewise the computed normalilzed co-spectral estimates (Figure 8) are in good overall agreement with the H_2O and CO_2 co-spectra out to a frequency of $n = 0.2$ Hz. At higher frequencies, the normalized CH_4 co-spectra are systematically lower than the estimates from the infrared gas analyzer. In part this roll-off of the power and co-spectra is due to the effects of the 0.1 s time constant on the phase and amplitude of the instantaneous methane concentration. In addition to the electronic roll-off, the larger sampling volume of the CH_4 sensor and greater displacement from the sonic anemometer (compared to the infrared gas analyzer) will cause roll-off at high frequencies. Using the methodology outlined by Moore (1986), an estimate of the flux loss as a result of path averaging and lateral sensor separation can be made. The fractional flux loss ($\Delta F/F$) is determined as

$$\frac{\Delta F}{F} = 1 - \frac{\int_0^\infty T_{\mathrm{wc}}(n) C_{\mathrm{wc}}(n) \mathrm{d}n}{\int_0^\infty C_{\mathrm{wc}}(n) \mathrm{d}n}, \tag{7}$$

where n is the frequency, C_{wc} is the co-spectral density, and T_{wc} is the transfer function with values between 0 and 1 that characterizes the effect of path averaging (for the velocity and scalar sensors) and the resulting flux loss due to lateral separation of the sensors. Equations describing the transfer functions for these effects are described in detail by Moore (1986). With a physical path length of 0.5 m, a lateral separation of 0.7 m from the vertical velocity sensor, and a measurement height of 2.5 m above ground level, the estimated flux loss is 18% for the CH_4 sensor. At a measurement height of 10 m, the expected flux loss would be 7%. A measurement height of 2.5 m was chosen at this site to keep the expected flux 'footprint' within the landfill area (Schuepp *et al.*, 1990).

Since the area under the co-spectral curves in Figure 8 represents the flux, an estimate of flux loss can also be obtained by comparing integrated co-spectra in a specified frequency range with results from the H_2O/CO_2 sensor. Assuming the H_2O and CO_2 co-spectra approximate those for an ideal sensor, the normalized spectral fractions (f/F) are computed as

$$\frac{f}{F} = \frac{\int_0^{n_1} C_{\mathrm{wc}}(n) \mathrm{d}n}{\int_0^\infty C_{\mathrm{wc}}(n) \mathrm{d}n}. \tag{8}$$

A higher spectral fraction of CH_4 compared to that from an ideal sensor indicates some flux loss. A value of 0.2 was selected for n_1 because of the good agreement in all the co-spectral estimates to a frequency of $n = 0.2$. The computed spectral fractions for H_2O and CO_2 were nearly identical. For CH_4, the spectral fraction was higher, indicating some flux loss. To make the CH_4 spectral fraction equal to that obtained for the H_2O and CO_2 fraction, the total flux had to be increased by 15%. This method of estimating the flux loss includes both geometric and electronic filtering effects, and is consistent with flux loss as estimated from the measurement geometry.

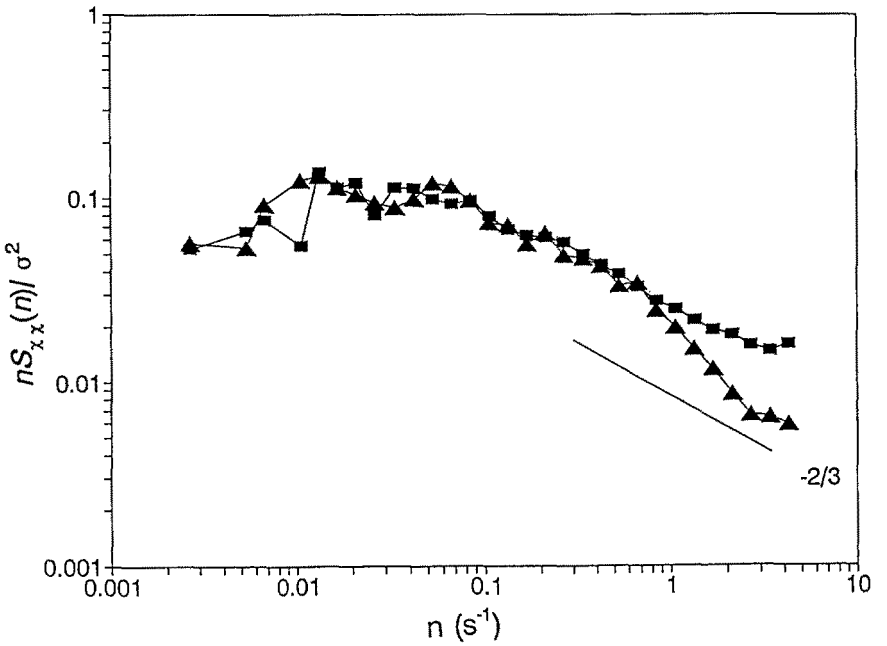

Fig. 7. Power spectra ($S_{\chi\chi}$) of H_2O (■) and CH_4. (△). Power spectra are multiplied by frequency (n) and divided by the variance to make the area under the curve equal to 1.

3.4. CH_4 FLUX RESOLUTION

Random instrument noise can increase the variance of scalar fluxes measured for a finite sampling period. This is in addition to the normal run-to-run variability experienced using ideal sensors under the best conditions. Lenschow and Kristensen (1985) determined that the error variance of a scalar flux (F_s) for typical atmospheric turbulent variations over a period T is

$$\sigma^2(F,\ T) \approx 4\sigma_s^2\sigma_w^2 \frac{\min(\Gamma_s,\ \Gamma_w)}{T}\ , \tag{9}$$

where Γ_s and Γ_w are the integral time scales of scalar s and vertical velocity w; the noise free variance of the scalar is given by (σ_s^2). Using the expressions derived by Lenschow and Kristensen (1985), Ritter *et al.* (1990) assessed the percentage of the error variance due to sensor noise. They estimate the total error variance as

$$\sigma^2(F,\ T) \approx \frac{\sigma_w^2}{T}(4\sigma_s^2\Gamma_w + \sigma_n^2\Delta t)\ , \tag{10}$$

where σ_n^2 is the sensor noise variance and Δt is the sampling interval. Our sensor has a noise level of about 65 ppb CH_4. For a methane emission rate of 10 mmol m^{-2} hr^{-1}, the noise variance constitutes 20% of the total error variance for the flux. For a flux of 0.1 mmol m^{-2} hr^{-1}, the noise variance comprises nearly 95% of

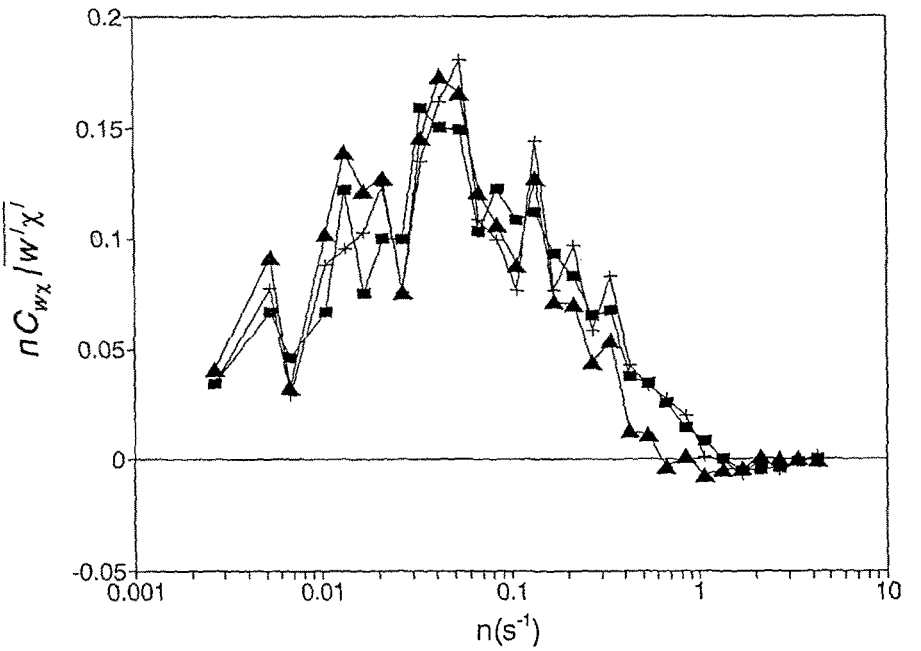

Fig. 8. Co-spectra ($C_{w\chi}$) for H_2O (■), CO_2 (+), and CH_4 (△) as a function of frequency. The co-spectral estimates are multiplied by frequency and normalized by the flux so that the area under the curve is equal to 1.

the total error variance. After integrating data for one hour, the standard deviation when measuring small fluxes ($\lesssim$ 0.1 mmol m^{-2} hr^{-1}) is expected to be 0.05 mmol m^{-2} hr^{-1} (20 mg m^{-2} d^{-1}).

4. Summary

In laboratory tests, the prototype methane sensor demonstrated adequate sensitivity for measuring by eddy correlation fluxes greater than 0.05 mmol m^{-2} hr^{-1}. Higher sensitivity can be achieved by reducing the effects of baseline offsets in the optical path. In field tests, the CH_4 sensor showed both adequate frequency response and sensitivity. The estimated flux loss due to path averaging when operated at a height of 2.5 m above ground level was about 15%. Systematic errors due to the effects of temperature fluctuations on the spectroscopic properties of methane were estimated. Proper choice of the modulation amplitude should reduce these systematic errors to 0.025 mmol m^{-2} hr^{-1}. Ongoing work is aimed at quantifying various error sources, developing a more rugged instrument, stabilizing the optical alignment, and simplifying the electronic signal processing circuitry.

On November 23 1991, we measured CH_4 emission rates from a clay-capped sanitary landfill near Oak Ridge. TN, at which no gas recovery system was implemented. The average uncorrected flux, 17 mmol m^{-2} h^{-1} (6400 mg m^{-2} d^{-1}),

falls within the range reported for landfills as determined by soil diffusion, and is about 30 times smaller than the flux reported from a landfill in Tokyo bay. Our reported flux is 20 to 200 times larger than that expected from natural methanogenic ecosystems; the improvements outlined above should permit us to quantify fluxes from many such ecosystems. The flux mole ratio of CH_4/CO_2 was about 2 : 1 and is consistent with biogas mole ratios measured elsewhere. Exercise caution when evaluating the role of landfills in the global CH_4 budget based on this study: the test runs reported here reflect a small sampling in space and time. However, the large fluxes reported here do affirm the significance of landfills as an important source of atmospheric methane.

Acknowledgements

We thank Iris Shelton for her assistance in coordinating the experiment with the Oak Ridge Y-12 Plant operations management. Chris Hovde and Alan Stanton acknowledge support from the U.S. Department of Energy under Grant No. DE-FG03-90ER81053.

References

Allan, D. W., 1966, Statistics of atomic frequency standards, Proc. IEEE **54**, 221–230.

Anderson, S. M. and Zahniser, M. S., 1991, Open-path tunable diode laser absorption for eddy correlation flux measurements of atmospheric trace gases, in H. I. Schiff (ed.), *Measurement of Atmospheric Gases*, Proc. SPIE 1433, 167–178.

Arndt, R., 1965, Analytical line shapes for Lorentzian signals broadened by modulation, *J. Appl. Phys.* **36**, 2522–2524.

Auble, D. L. and Meyers, T. P., 1992, An open path, fast response infrared absorption gas analyzer for H_2O and CO_2, *Boundary-Layer Meteorol.* **59**, 243–256.

Baldocchi, D. D., Hicks, B. B., and Meyers, T. P., 1988, Measuring biosphere-atmosphere exchanges of biologically related gases with micrometeorological methods, *Ecology* **69** (5), 1331–1340.

Bingemer, H. G. and Crutzen, P. J., 1987, The production of methane from soil wastes, *J. Geophys. Res.* **92** (D2), 2181–2187.

Bobin, B., 1972, Interpretation de la bande harmonique $2\nu_3$ du methane $^{12}CH_4$ (de 5890 a 6107 cm^{-1}), *J. Physique* **33**, 345–352.

Bogner, J. E. and Vogt, M. C., 1991, Methane emissions from sanitary landfills, Argonne National Laboratory, Argonne, Illinois, NTIS Document No. DE91-010652.

Bomse, D. S., Stanton, A. C. and Silver, J. A., 1992, Frequency modulation and wavelength modulation spectroscopies: comparison of experimental methods using a lead-salt diode laser, *Appl. Opt.* **31**, 718–731.

Bomse, D. S., 1991, Dual-modulation laser line-locking scheme, *Appl. Opt.* **30**, 2922–2924.

Businger, J. A., 1986, Evaluation of the accuracy with which dry deposition can be measured with current micrometeorological techniques, *J. Climate Appl. Meteorol.* **25**, 1100–1124.

Cassidy, D. T. and Reid, J., 1982, Harmonic detection with tunable diode lasers – two-tone modulation, *Appl. Phys. B.* **29**, 279–285.

Cicerone, R. J. and Oremland, R. S., 1988, Biogeochemical aspects of atmospheric methane, *Global Biogeochem. Cycles* **2**, 299–328.

Cooper, D. E. and Carlisle, C. B., 1988, High sensitivity FM spectroscopy with a lead-salt diode laser, *Opt. Lett.* **13**, 719–721.

Crutzen, P. J., 1991, Methane's sinks and sources, *Nature* **350**, 380–381.

Darnton, L. and Margolis, J. S., 1973, The temperature dependence of the half widths of some self- and foreign-gas-broadened lines of methane, *J. Quant. Spectrosc. Radiat. Transfer* **13**, 969–976.

Fan, S. M., Wofsy, S. C., Bakwin, P. S., Jacob, D. J., Anderson, S. M., Kebabian, P. L., McManus, J. B., and Kolb, C. E., 1992, Micrometeorological measurements of CH_4 and CO_2 exchange between the atmosphere and subarctic tundra, *J. Geophys. Res.* **97**, 16,627–16,643.

Fox, K., Halsey, G. W., Daunt, S. J., Blass, W. E., and Jennings, D. E., 1980, Anomalous $^{13}CH_4$: $^{12}CH_4$ line strengths in $2\nu_3$, *J. Chem. Phys.* **72**, 4657–4659.

Herriott, D. R., Kogelnik, H., and Kompfner, R., 1964, Off-axis paths in spherical mirror interferometers, *Appl. Opt.* **3**, 523–526.

Hastie, D. R., Mackay, G. I., Iguchi, T., Ridley, B. A., Schiff, H. I., 1983, Tunable diode laser systems for measuring trace gases in tropospheric air, *Environ. Sci. and Technol.* **17**, 352A–364A.

Hicks, B. B., Matt, D. R., and McMillen, R. T., 1989, A micrometeorological investigation of surface exchange of O_3, SO_2 and NO_2: A case study, *Boundary-Layer Meteorol.* **47**, 321–336.

Kaimal, J. C., Gaynor, J. E., Zimmerman, H. A., and Zimmerman, G. A., 1990, Minimizing flow distortion errors in a sonic anemometer, *Boundary-Layer Meteorol.* **53**, 103–115.

Khalil, M. A. K. and Rasmussen, R. A., 1990, Constraints on the global sources of methane and an analysis of recent budgets, *Tellus* **42B**, 229–236.

Lenschow, D. and Kristensen, L., 1985, Uncorrelated noise in turbulence measurements, *J. Atmos. Ocean. Tech.* **2**, 68–81.

Lubken, F.-J., Eng, R., Karecki, D. R., Mackay, G. I., Nadler, S., and Schiff, H. I., 1991, The effect of water vapour broadening on methane eddy correlation flux measurements, *J. Atmos. Chem.* **13**, 97–108.

Margolis, J. S., 1973, Line strength measurements of the $2\nu_3$ band of methane, *J. Quant. Spectrosc. Radiat. Transfer* **13**, 1097–1103.

McManus, J. B., Kebabian, P. L., and Kolb, C. E., 1989, Atmospheric methane measurement instrument using a Zeeman-split He-Ne laser, *Appl. Opt.* **28**, 5016–5023.

Mohebati, A. and King, T. A., 1988, Remote detection of gases by diode laser spectroscopy, *J. Mod. Optics* **35**, 319–324.

Moore, T. R. and Roulet, N. T., 1991, A comparison of dynamic and static chambers from methane emission measurements from subarctic fens, *Atmosphere-Ocean* **29(1)**, 102–109.

Moore, T. R. and Knowles, R., 1990, Methane emissions from fen, bog, and swamp peatlands in Quebec, *Biogeochemistry* **11**, 45–61.

Moore, C. J., 1986, Frequency response corrections for eddy correlation systems, *Boundary-Layer Meteorol.* **37**, 17–35.

Ritter, J. A., Lenschow, D., Barrick, J. D. W., Gregory, G., Sachse, G. W., Hill, G., and Woerner, M., 1990, Airborne flux measurements and budget estimates of trace species of the Amazon Basin during the GTE/ABLE 2B Expedition, *J. Geophys. Res.* **95**, 16,785–16,886.

Ritter, J. A., Barrick, J. D. W., Sachse, G. W., Hill, G. F., Gregory, G. L., Woerner, M. A., and Watson, C. E., 1992, Airborne flux measurements of trace gas species in an Arctic boundary layer, *J. Geophys. Res.* **97**, 16601.

Sachse, G. W., Collins, J. E. Jr., Hill, G. F., Wade, L. O., Burney, L. G., and Ritter, J. A., 1991, Airborne tunable diode laser sensor for high-precision concentration and flux measurements of carbon monoxide and methane, in H. I. Schiff (ed.), *Measurement of Atmospheric Gases*, Proc. SPIE 1433, 157–166.

Sarangi, S. and Varanasi, P., 1974, Measurement of intensities of multiplets in the $2\nu_3$-band of methane at low temperatures, *J. Quant. Spectrosc. Radiat. Transfer* **14**, 365–376.

Sass, R. L., Fisher, F. M., and Harcombe, P. A., 1990, Methane production and emission in a Texas rice field, *Global Biogeochemical Cycles*, **4(1)**, 47–68.

Schuepp, P. H., Leclerc, M. L., MacPherson, J. I., and Desjardins, R. L., 1990, Footprint predictions of scalar fluxes from analytical solutions of the diffusion equation, *Boundary-Layer Meteorol.* **50**, 355–373.

Senior, E. and Kasali, G. B., 1990, Landfill gas, in E. Senior (ed.), *Microbiology of Landfill Sites*, CRC Press, Boca Raton, Florida.

Shimose, Y., Okamoto, T., Maruyama, A., Aizawa, M., and Nagai, H., 1991, Remote sensing of methane gas by differential absorption using a wavelength tunable DFB LD, *IEEE Photon. Technol. Lett.* **3**, 86–87.

Silver, J. A. and Stanton, A. C., 1988, Optical interference fringe reduction in laser absorption experiments, *Appl. Opt.* **27**, 1914–1917.

Silver, J. A., 1992, Frequency-modulation spectroscopy for trace species detection: Theory and comparison among experimental methods, *Appl. Opt.* **31**, 707–717.

Stanton, A. C. and Hovde, D. C., 1992, *Laser Focus World*, August issue, 117–120.

Tohjima, Y. and Wakita, H., 1993, Estimation of methane discharge from a plume: A case of landfill, *Geophys. Res. Lett.* **20**, 2067–2070.

Uehara, K. and Tai, H., 1992, Remote detection of methane with a 1.66 μm diode laser, *Appl. Opt.* **31**, 809–814.

Varanasi, P., 1971, Collision-broadened half-widths and shapes of methane lines, *J. Quant. Spectrosc. Radiat. Transfer* **11**, 1711–1724.

Verma, S. B., Ullman, F. G., Billesbach, D., Clement, R. J., and Kim, J., 1992, Eddy correlation measurements of methane flux in a northern peatland ecosystem, *Boundary-Layer Meteorol.* **58**, 289–304.

Webb, E. K., Pearman, G. I., and Leuning, R., 1980, Correction of flux measurements for density effects due to heat and water vapour transfer, *Q. J. R. Meteorol. Soc.* **106**, 85–100.

Webster, C. R., 1985, Brewster-plate spoiler: A novel method for reducing the amplitude of interference fringes that limit tunable laser absorption, *J. Opt. Soc. Am. B* **2**, 1464–1470.

Werle, P., Josek, K., and Slemr, F., 1991, Application of FM spectroscopy in trace gas monitoring: A study of some factors influencing the instrument design, in H. I. Schiff (ed.), *Measurement of Atmospheric Gases*, Proc. SPIE 1433, 128–135.

Zahniser, M. S., Kebabian, P. L., Anderson, S., Freedman, A., and Kolb, C. E., 1987, IR laser absorption eddy correlation measurement devices for trace atmospheric gases, *AIP Conf. Proc.* **160**, 690–692.